Effects of Magnetic Order on the Superconducting Length Scales and Critical Fields in Single Crystal $ErNi_2B_2C$

P. L. Gammel, B. P. Barber, A. P. Ramirez, C. M. Varma, and D. J. Bishop
Bell Labs, Lucent Technologies, 700 Mountain Ave., Murray Hill, New Jersey 07974

P. C. Canfield and V. G. Kogan
Ames Laboratory and Department of Physics and Astronomy, Iowa State University, Ames, Iowa 50011

M. R. Eskildsen, N. H. Andersen, and K. Mortensen
Risø National Laboratory, P.O. Box 49, DK-4000 Roskilde, Denmark

K. Harada
Advanced Research Laboratory, Hitachi, Ltd., Hatoyama, Saitama 350-03 Japan
(Received 12 June 1998; revised manuscript received 26 October 1998)

The flux line form factor in small angle neutron scattering and transport data determines the superconducting length scales and critical fields in single crystal $ErNi_2B_2C$. For $H \parallel c$, the coherence length ξ increases and the penetration depth λ decreases when crossing $T_N = 6.0$ K, the Néel transition. The critical fields show corresponding anomalies near T_N. For $H \perp c$, the fourfold modulation of the upper critical field H_{c2} is strongly temperature dependent, changing sign near T_N, and can be modeled using the anisotropy of the sublattice magnetization. [S0031-9007(99)08514-2]

PACS numbers: 74.60.Ec, 74.25.Dw, 74.25.Ha

A rich vehicle for studying the interplay between superconductivity and magnetism is the $(RE)Ni_2B_2C$ system [1], with T_N/T_c varying from 0.14(RE = Tm) to 1.6(RE = Dy) across the rare earth series [2]. This range means that the salient energy scales for antiferromagnetic order and superconductivity can be explored in both limits $T_c < T_N$ and $T_c > T_N$. For $T_c > T_N$, the antiferromagnetic transition occurs within the superconducting state. In this case, it is interesting to examine the interplay between superconductivity and magnetism in the critical regime near T_N. Fundamental to this interplay and, indeed, to understanding the superconducting state in general, are the superconducting length scales: The coherence length ξ, the penetration depth λ, and the superconducting critical fields, including the lower critical field H_{c1}, the upper critical field H_{c2}, and the thermodynamic critical field H_c.

In magnetic superconductors, however, only H_{c2} can be easily measured using transport data [3]. Magnetization and specific heat data, used to determine H_{c1} and H_c, are typically dominated by the response of the magnetism, particularly in large moment systems such as $(RE)Ni_2B_2C$.

In this Letter, we have studied single crystal $ErNi_2B_2C$ [4], a strongly type-II ($\kappa \sim 5$) superconductor with $T_c = 10.5$ K and, well below T_c, a magnetic transition [5] at $T_N = 6.0$ K, in an incommensurate, transversely polarized spin density wave with $q = 0.5526a^*$. For strongly type-II superconductors, most of the H-T plane is occupied by the mixed state, wherein the material is permeated by an array of quantized flux lines. In the mixed state, the superconducting properties are controlled by the flux-line lattice (FLL). Small-angle neutron scattering (SANS) experiments separate superconductivity, via the FLL periodicity, and the magnetic order, with a typically much smaller periodicity than the FLL, in reciprocal space, allowing them to be studied independently. The intensity of the FLL Bragg reflections is determined by the structure of the individual flux line through the form factor. This form factor involves the superconducting penetration depth λ, which determines the range of the magnetic field around an isolated flux line, and the coherence length ξ, which determines the size of the core of a flux line. Using these independently measured length scales we have calculated the critical fields H_{c1}, H_{c2}, and H_c. For fields $H \parallel c$, all of these data show distinct signatures on crossing through T_N. We have made a comparison of the change in H_c to the predictions of a weak critical divergence of the pair breaking parameter. For $H \perp c$, we have studied and modeled the influence of the magnetic order on the in-plane anisotropy of H_{c2}.

Our sample was a single crystal [4] of $ErNi_2B_2C$ incorporating B^{11} to enhance neutron transmission. The sample was an irregular platelet 1.3-mm thick and approximately 11×8 mm in size. For the neutron experiments, the sample edges were masked with Cd, leaving a rectangular region 10×7 mm exposed. The FLL was imaged [6] using the SANS instrument at Risø National Laboratory. Briefly, a magnetic field is applied roughly parallel to the incident neutron beam, whose wavelength is $6 < \lambda_n < 11$ Å. The neutrons are Bragg scattered from the magnetic field pattern of the FLL and counted by an area detector at the end of a 6 m evacuated chamber. For $H \parallel c$ the FLL was square over the range of this study,

 0031-9007/99/82(8)/1756(4)$15.00

$H = 1-10$ kOe and $T = 3-8.5$ K. In this case, the reflectivity of the first order FLL Bragg peaks, calculated from Ginzburg-Landau (GL) corrections to the London model [6], is $R = (2\pi\gamma_n 2t/16\phi_0^2 q)H_1^2$, where γ_n is the neutron gyromagnetic ratio and t is the sample thickness. The flux-line structure contributes to the reflectivity through the form factor $H_1 = (\phi_0/\lambda^2)(\frac{1}{4}\pi^2)\exp(-2\pi^2 B\xi^2/\phi_0)$. Our data consist of the field dependence of R, averaged over four first order reflections, which we used in conjunction with the reflectivity formulas to determine $\lambda(T)$ and $\xi(T)$ as shown in Fig. 1. The low temperature results, $\lambda \sim 700$ Å and $\xi \sim 150$ Å, agree with the literature [4,6]. Both parameters show pronounced features near T_N.

Near a magnetic transition, one expects λ to be reduced by both the susceptibility [7] as $\lambda \sim \lambda_0/(1 + 4\pi\chi)^{1/2}$ and the mean free path ℓ as $\lambda \approx \lambda_0(1 + \xi_0/\ell)^{1/2}$. Neither effect, however, explains our data. First, published data [4,5] for the susceptibility χ give a result over an order of magnitude too small to account for the feature in our data. Second, normal state transport data show [4] only a smooth evolution of ℓ, it being temperature independent above T_N and gradually increasing by 30% below T_N. This does not, then, explain our sharp features near T_N. The coherence length $\xi(T)$ is similarly affected [8] by ℓ as $\xi^{-1} = \xi_0^{-1} + \ell^{-1}$. Again, this expression does not account for our data near T_N.

We have used the length scales measured in our SANS experiment to calculate all of the superconducting critical fields. First, the upper critical field is calculated using $H_{c2} = \phi_0/2\pi\xi^2$ as shown by the open triangles in Fig. 2. The solid line is the transport data [4], using pieces cut from the same sample and an onset resistance criterion. Above T_N, the two types of data to determine H_{c2} coincide exactly. Near T_N, both types of data show a comparable drop in H_{c2}, but the SANS data increase more strongly at low temperatures. The difference in these two measures in the magnetically ordered state is still unclear. However, there is a change in the shape of the resistance isotherms used to determine H_{c2} below T_N, which may, in part, account for this discrepancy. Second, we have calculated the lower critical field from $H_{c1} = (\phi_0/4\pi\lambda^2)[\ln\kappa + 0.5]$ as shown by the open squares in Fig. 2. As stated in the introduction, these are the first data on H_{c1} in this system. To simplify Fig. 2, we have omitted error bars on the H_{c1} data, which are comparable in relative magnitude to those shown for H_{c2}. The decrease in λ is the dominant contribution to H_{c1} near T_N, giving rise to the upward cusp in our data. We can also combine the data on λ and ξ to determine the dimensionless Ginzburg-Landau parameter $\kappa = \lambda/\xi$ as shown in the top panel in Fig. 3. This value has a remarkable temperature dependence, dropping more than 20% near T_N, and also assuming a generally lower value in the magnetically ordered state.

The thermodynamic critical field H_c is one of the most fundamental properties of the superconducting state, as it can be related either to the difference in the free energies between the normal and superconducting states or to the superconducting energy gap $\Delta(T)$. We have measured both magnetization and specific heat on this sample, but determination of H_c in these experiments was inconclusive in the presence of the magnetic signal. This underscored the unique role of SANS data in understanding the thermodynamic aspects of the interplay of superconductivity and magnetism. The diamonds in the bottom panel of Fig. 3 show the SANS data for the thermodynamic critical field using the GL formula $H_c(T) = \phi_0/[2\sqrt{2}\,\pi\xi(T)\lambda(T)]$.

Our data for H_c show a pronounced reduction near T_N. In the inset of Fig. 3, this region is shown in an expanded scale. The dashed line, which accurately describes the data in the paramagnetic regime, is the mean field result [8], $H_c(T) = H_c(T = 0)[1 - (T/T_c)^2]$. Reductions in H_c near magnetic transitions were previously treated theoretically [9] from the standpoint of pair breaking. Near T_N, one generically expects magnetic fluctuations to

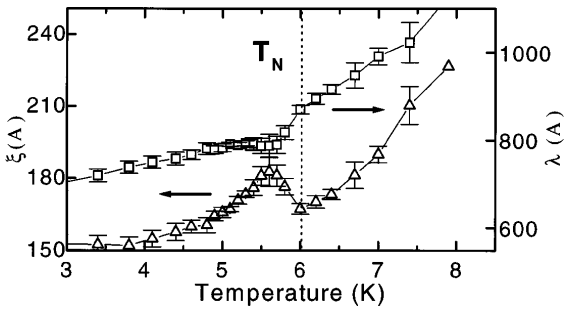

FIG. 1. Shown are the temperature dependence of λ, the superconducting penetration depth (□), and ξ, the superconducting coherence length (△), as measured using the flux line form factor in a SANS experiment. Both quantities show distinct features near T_N.

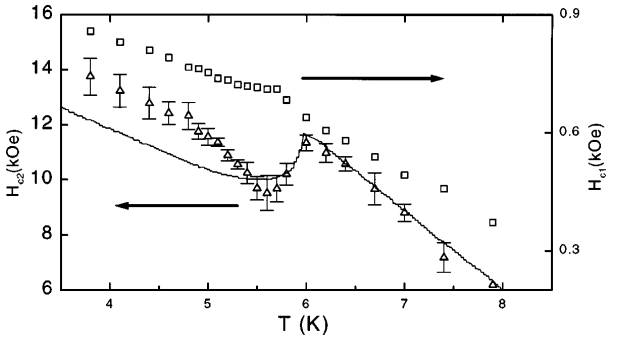

FIG. 2. Shown are the temperature-dependent superconducting critical fields H_{c2} and H_{c1}. The upper critical field H_{c2} (△) determined from the SANS data using $H_{c2} = \phi_0/2\pi\xi^2$ agrees exactly with transport data (line) above T_N, but shows some deviations in the ordered state. The lower critical field H_{c1} (□) defined by $H_{c1} = (\phi_0/4\pi\lambda^2)[\ln\kappa + 0.5]$ shows a slight increase near T_N.

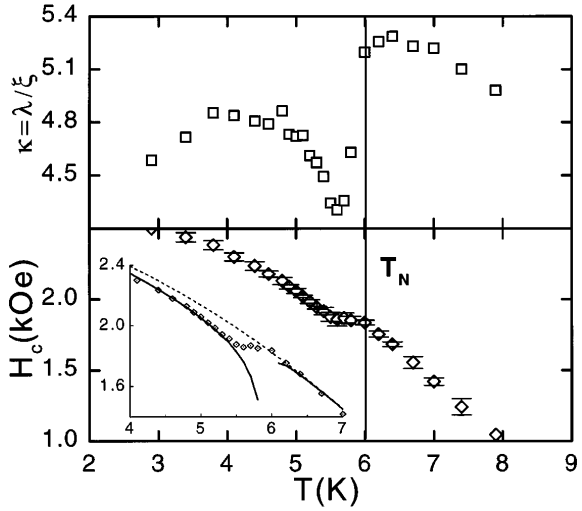

FIG. 3. Top: shown is $\kappa = \lambda/\xi$ from the SANS data, which shows a strong reduction near T_N, and an overall reduction in the magnetically ordered state. Bottom: shown is the thermodynamic critical field $H_c(T) = \phi_0/[2\sqrt{2}\,\pi\xi(T)\lambda(T)]$ determined from the SANS data, which should not be affected by changes in the transport mean free path. In the inset, the region near T_N is expanded and two fits are shown. The dashed line is the mean field result, which accurately describes the data above T_N. The solid line includes the theoretically predicted correction due to the weak divergence of the pair breaking parameter ρ.

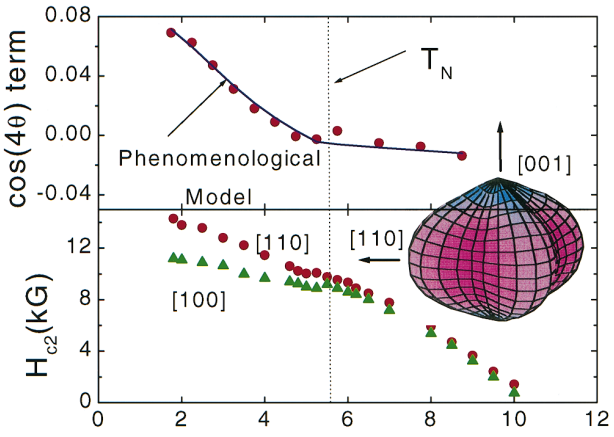

FIG. 4(color). Shown is the anisotropy of the upper critical field for $H \perp c$ from transport data. In the lower panel are rough data along two principal directions. These data are marred by misalignment relative to the c axis. Shown in the inset is the full solid body rotation data for H_{c2} at $T = 2$ K, with the in-plane oscillations magnified for clarity. In the upper panel, the open circles are fits to the fourfold in-plane component $H_{c2}(\theta) = H_{c2}[1 + \gamma\cos(4\theta)]$. The solid line is the phenomenological model described in the text.

increase the pair breaking parameter ρ. For the case of partial Fermi surface nesting, the detailed prediction [9] is a weak critical divergence $\rho = \rho(T = 0) + \Delta\rho[(T - T_N)/T_N]^{\alpha-1}$, where α is the specific heat exponent. Since our data are rounded near T_N, we fix $\alpha = 0.13$, the 3D Ising value [10]. For weak pair breaking [11], the effect on the critical field is in the prefactor, with $H_{c0}(T = 0)/H_c(T = 0) = 1 - 0.57\pi^2\rho$, where we use H_{c0} to denote values below T_N. We normalize taking $H_c(T = 0)$ from the data above T_N and combine all of the above formulas to get the solid lines in the inset. To get a good fit to the data, we have set the amplitude $\Delta\rho$ of the divergent contribution to the pair breaking to be a factor of 10 larger below T_N than above. Outside of a rounded region with 0.5 K of the Néel transition, the fit is quite good. This rounding is about the same as in measurements [5] of the magnetic order. These data, and specifically the divergent component of ρ, are the first measurements of pair breaking near a magnetic transition.

For fields $H \perp c$, H_{c2} was determined from transport data. Small-angle neutron scattering experiments in this geometry were obscured by the Er absorption cross section and the crystal geometry, so only H_{c2} could be determined. Data for the field along two principal directions in the plane, [100] and [110], are shown in the lower panel of Fig. 4. These results were found not to depend on the direction of the transport current in this geometry. For fields perpendicular to c, T_N is reduced by about 0.5 K at H_{c2} [4]. $ErNi_2B_2C$ is a tetragonal crystal, so the leading order correction to H_{c2} in the a-b plane is of the form $\cos(4\theta)$, where θ is the angle in the plane. The $\cos(4\theta)$ term, if it has sufficient magnitude, will stabilize [12] a square FLL in the vicinity of H_{c2}.

To understand this term in more detail, we used a two-axis platform to perform full solid body rotations of the field while measuring H_{c2}. An example of such data at $T = 2$ K is shown in the inset of Fig. 4, where the in-plane oscillations have been magnified for clarity. In addition to the in-plane oscillations we describe here, note that H_{c2} shows a distinct cusp along the c axis, which we were unable to understand within a simple effective mass approximation [13]. Two ac current directions, $I \parallel a$ and $I \angle (45°)$, were used and found not to influence H_{c2}. However, precise alignment relative to the field *is* extremely important as the 40% greater H_{c2} in the c direction produces a $\cos(2\theta)$ term which can dominate the 10% in plane anisotropy when the sample is only aligned by eye at room temperature. Shown in the top half of Fig. 4 is the expansion coefficient $H_{c2} = H_{c2,0}[1 + \gamma\cos(4\theta)]$ extracted from the solid body rotations. Note, first, the term is strongly temperature dependent below T_N. Second, γ actually changes sign near T_N.

We describe the effect of magnetic order on the H_{c2} anisotropy using a simple phenomenological model. Superconductivity disappears due to a net internal field $B_{c2}(T)$, which is related to the external field via $H_{c2}(T) = B_{c2}(T) - 4\pi M(T, \theta)$. $B_{c2}(T)$ does not depend on any anisotropy due to the magnetic order, and, for fields in the basal plane, normal state rotation data imply that B_{c2} does not have any $\cos(4\theta)$ anisotropy. In the expression for

H_{c2}, M is the uniform magnetization induced by rotating the sublattice magnetization through an angle φ, i.e., $M = 2M_s \sin(\varphi)$. We first find a relation between θ and φ by minimizing the free energy

$$F = \alpha M^2/2 + \tfrac{1}{4}[\beta_1 + \beta_2 \sin 4(\varphi)]M^4 - \mathbf{M} \cdot \mathbf{H} \quad (1)$$

with respect to φ using the above expression for M. Here α and the β's are all positive. Calculating φ and adding the contributions of the two orthogonal domains which are present in these twinned samples below T_N, we find

$$H_{c2}(\theta, T) = B_{c2}(T) - \alpha_0 H_{c2}(\theta, T) + (\beta_0/\alpha^3) H_{c2}^3(T, \theta) \cos(4\theta), \quad (2)$$

where α_0 and β_0 are simply related to the coefficients in (1). Assuming small rotation φ, or, equivalently, small additional anisotropy, $H_{c2}(T, \theta)$ in the right-hand side of Eq. (2) may be replaced by $B_{c2}(T)$. Then the leading anisotropy term is proportional to $B_{c2}^3(T) \cos(4\theta)$. In the top panel of Fig. 4, we show the fit to this form over the entire temperature range, although the derivation is strictly valid only below T_N. Clearly, we get an excellent fit with the overall magnitude used as a free parameter. In principle, further measurements of the anisotropic magnetic susceptibility below T_N should allow comparison of the magnitude as well.

In conclusion, we have made the first detailed measurement of the superconducting length scales and critical fields in a magnetic superconductor through the Néel transition using SANS and transport studies of single crystal $ErNi_2B_2C$. All of the measured quantities show distinct anomalies near T_N. While much remains to be understood about these effects, they underscore the interplay between superconductivity and magnetism in this system. We have, however, made a preliminary analysis of the reduction in the thermodynamic critical field near T_N. These data show the predicted weak divergence of the pair breaking parameter near T_N. We have also seen how the antiferromagnetic order changes the in-plane fourfold modulation of H_{c2}, which affects the stability of the ubiquitous [14] square FLL seen in these compounds.

[1] P. C. Canfield, P. L. Gammel, and D. J. Bishop, Phys. Today **51**, No. 10, 40–46 (1998).

[2] B. K. Cho, P. C. Canfield, and D. C. Johnston, Phys. Rev. B **52**, R3844 (1995).

[3] H. C. Hamaker *et al.*, Solid State Commun. **32**, 289 (1979); Ø. Fischer *et al.*, J. Phys. (Paris) **40**, C5–89 (1979); G. Zwicknagl and P. Fulde, Z. Phys. B **43**, 23 (1981).

[4] B. K. Cho *et al.*, Phys. Rev. B **52**, 3684 (1995).

[5] J. Zarestky *et al.*, Phys. Rev. B **51**, 678 (1995); S. K. Sinha *et al.*, *ibid.* **51**, 681 (1995); J. W. Lynn *et al.*, Phys. Rev. B **55**, 6584 (1997).

[6] U. Yaron *et al.*, Nature (London) **382**, 236 (1996); M. R. Eskildsen *et al.*, Phys. Rev. Lett. **78**, 1968 (1997).

[7] K. E. Gray, Phys. Rev. B **27**, 4157 (1983).

[8] M. Tinkham, *Introduction to Superconductivity* (Krieger, Malabar, FL, 1980).

[9] T. V. Ramakrishnan and C. M. Varma, Phys. Rev. B **24**, 137 (1981). In Eq. (2.12), the exponent has a sign error. It should be $1 - \alpha$, not $\alpha - 1$.

[10] *Modern Theory of Critical Phenomena*, edited by S.-K. Ma (Benjamin-Cummings, Reading, MA, 1976), see table on p. 55.

[11] K. Maki, in *Superconductivity*, edited by R. D. Parks (Marcel Dekker, New York, 1969), pp. 1036–1105.

[12] Y. De Wilde *et al.*, Phys. Rev. Lett. **78**, 4273 (1997); K. Park and D. A. Huse, cond-mat/9804070.

[13] P. L. Gammel *et al.*, Phys. Rev. Lett. **72**, 278 (1994); L. Campbell *et al.*, Phys. Rev. B **38**, 2439 (1988); L. L. Daemon, L. J. Campbell, and V. G. Kogan, Phys. Rev. B **46**, 3631 (1992).

[14] M. Yethiraj *et al.*, Phys. Rev. Lett. **78**, 4849 (1997).